Rate-Dependent Carbon and Nitrogen Kinetic Isotope Fractionation in Hydrolysis of Isoproturon

ARTICLE *in* ENVIRONMENTAL SCIENCE AND TECHNOLOGY · DECEMBER 2008

Impact Factor: 5.33 · DOI: 10.1021/es801101c · Source: PubMed

3 AUTHORS:

Holger Penning
BASF SE
19 PUBLICATIONS **459** CITATIONS
SEE PROFILE

Christopher J Cramer
University of Minnesota Twin Cities
532 PUBLICATIONS **23,514** CITATIONS
SEE PROFILE

Martin Elsner
Helmholtz Zentrum München
87 PUBLICATIONS **2,045** CITATIONS
SEE PROFILE

Article

Rate-Dependent Carbon and Nitrogen Kinetic Isotope Fractionation in Hydrolysis of Isoproturon

Holger Penning, Christopher J. Cramer, and Martin Elsner

Environ. Sci. Technol., **2008**, 42 (21), 7764-7771 • DOI: 10.1021/es801101c • Publication Date (Web): 10 October 2008

Rate-Dependent Carbon and Nitrogen Kinetic Isotope Fractionation in Hydrolysis of Isoproturon

HOLGER PENNING,[†] CHRISTOPHER J. CRAMER,[‡] AND MARTIN ELSNER*,[†]

Institute of Groundwater Ecology, Helmholtz Zentrum München, German Research Center for Environmental Health, Ingolstädter Landstr. 1, 85764 Neuherberg, Germany, and Department of Chemistry and Supercomputing Institute, University of Minnesota, 207 Peasant St. SE, Minneapolis, Minnesota 55455-0431

Received April 22, 2008. Revised manuscript received September 5, 2008. Accepted September 8, 2008.

Stable isotope fractionation permits quantifying contaminant degradation in the field when the transformation reaction is associated with a consistent isotope enrichment factor ε. When interpreted in conjunction with dual isotope plots, isotope fractionation is also particularly useful for elucidating reaction mechanisms. To assess the consistency of ϵ and dual isotope slopes in a two-step reaction, we investigated the abiotic hydrolysis of the herbicide isoproturon (3-(4-isopropylphenyl)-1,1-dimethylurea) using a fragmentation method that allows measuring isotope ratios in different parts of the molecule. Carbon and nitrogen position-specific isotope fractionation, as well as slopes in dual isotope plots, varied linearly with rate constants k_{obs} depending on the presence of buffers that mediate the initial zwitterion formation. The correlation can be explained by two consecutive reaction steps (zwitterion formation followed by dimethylamine elimination) each of which has a different kinetic isotope effect and may be rate-limiting. Intrinsic isotope effects for both steps, extracted from our kinetic data using a novel theoretical treatment, agree well with values computed from density functional calculations. Our study therefore demonstrates that more variable isotope fractionation may be observed in simple chemical reactions than commonly thought, but that consistent ϵ or dual isotope slopes may nonetheless be encountered in certain molecular fragments.

Introduction

Compound specific isotope analysis (CSIA) may provide valuable information on the origin and fate of organic compounds in the environment. Substances are separated by gas chromatography, combusted online, and analyzed by isotope ratio mass spectrometry (GC-IRMS) making it possible to analyze small compound concentrations in environmental samples. Isotope ratios are thereby determined as average ("bulk") over the molecular structure of given target compounds. Compared to conventional methods, this approach delivers compound-specific information and provides improved sensitivity, yet does not yield the same level of mechanistic insight as position-specific isotope studies in chemistry. The method has been applied in biogeochemistry and environmental science, on the one hand to characterize sources of organic chemicals, and on the other hand, to trace their (bio)chemical degradation reactions through the enrichment of heavy isotopes caused by kinetic isotope effects (KIE) (*1*). Specifically, it has been possible to identify transformation pathways from characteristic regression slopes when isotopic changes for two elements were plotted in the same diagram (dual isotope, "2D", plots) (*2*−*5*). Even quantification of degradation has been accomplished, providing lines of evidence for the monitored natural attenuation of organic contaminants (*6*−*8*). This quantification is based on the Rayleigh equation and therein on the isotope enrichment factor ε_{bulk}, which must be determined experimentally and is a measure for the isotopic enrichment inside an organic compound (*1, 5, 7*). In order to identify and quantify natural transformation reactions for a given substance, constant slopes in a dual isotope plot, as well as consistent values of ε are, therefore, two prerequisites.

Recent research has addressed the robustness and variability of enrichment factors ϵ and 2D isotope slopes for different substances (*5, 9*−*12*). It is understood that observable fractionation may become small if transport or diffusion of substrate molecules becomes rate-limiting (*5, 13*). Enrichment factors ε may therefore show considerable variation, and if conservative estimates of ε are used, the true extent of degradation at contaminated sites can be underestimated. Since the preceding slow step is generally not fractionating, however, isotope effects of both elements are similarly affected (*5, 9*). In such a case, dual isotope plots show the same characteristic slope, and identification of transformation pathways is still possible (*3*−*5, 9, 14*).

This study investigates how ε values and 2D slopes are affected in a two-step reaction if not only one, but both reaction steps are associated with isotope fractionation. As a simple model system, we chose the abiotic hydrolysis of the herbicide isoproturon (3-(4-isopropylphenyl)-1,1-dimethylurea) at 60 °C. Mechanistic insight from previous studies (*15*−*20*) is summarized in the scheme of Figure 1. The presence of buffers BH (e.g., $H_2PO_4^-$, OH^- etc.) is hypothesized to catalyze an intramolecular proton transfer leading to formation of a short-lived zwitterionic intermediate (step 1) (*16*). Subsequently, this intermediate decomposes to 4-isopropylphenylisocyanate and dimethylamine in a reaction representing the first irreversible step of the reaction sequence (step 2). Even though the isocyanate is further hydrolyzed to CO_2 and the corresponding aniline, reaction kinetics, and therefore isotope effects depend only on these first two reaction steps. Reaction rates were found to vary between a minimum in the absence of buffers and at circumneutral pH—this is where only H_2O molecules can act as catalysts so that step 1 becomes partially rate-determining—and a maximum at pH ≤ 2, pH ≥ 12, or in the presence of high buffer concentrations—this is where H_3O^+, OH^-, or buffer molecules effectively catalyze step 1. Further increase in pH or buffer concentration did not lead to additional rate acceleration indicating that under these conditions, step 2 is rate-determining (*16*).

To investigate how this affects measurable isotope fractionation, the herbicide isoproturon is particularly suited as a model compound. With our recently developed GC-IRMS method (*21*), this substance can be decomposed into

* Corresponding author phone: +49-89-31872565; fax: +49-89-31873361; e-mail: martin.elsner@helmholtz-muenchen.de.
[†] German Research Center for Environmental Health.
[‡] University of Minnesota.

10.1021/es801101c CCC: $40.75

Published on Web 10/10/2008

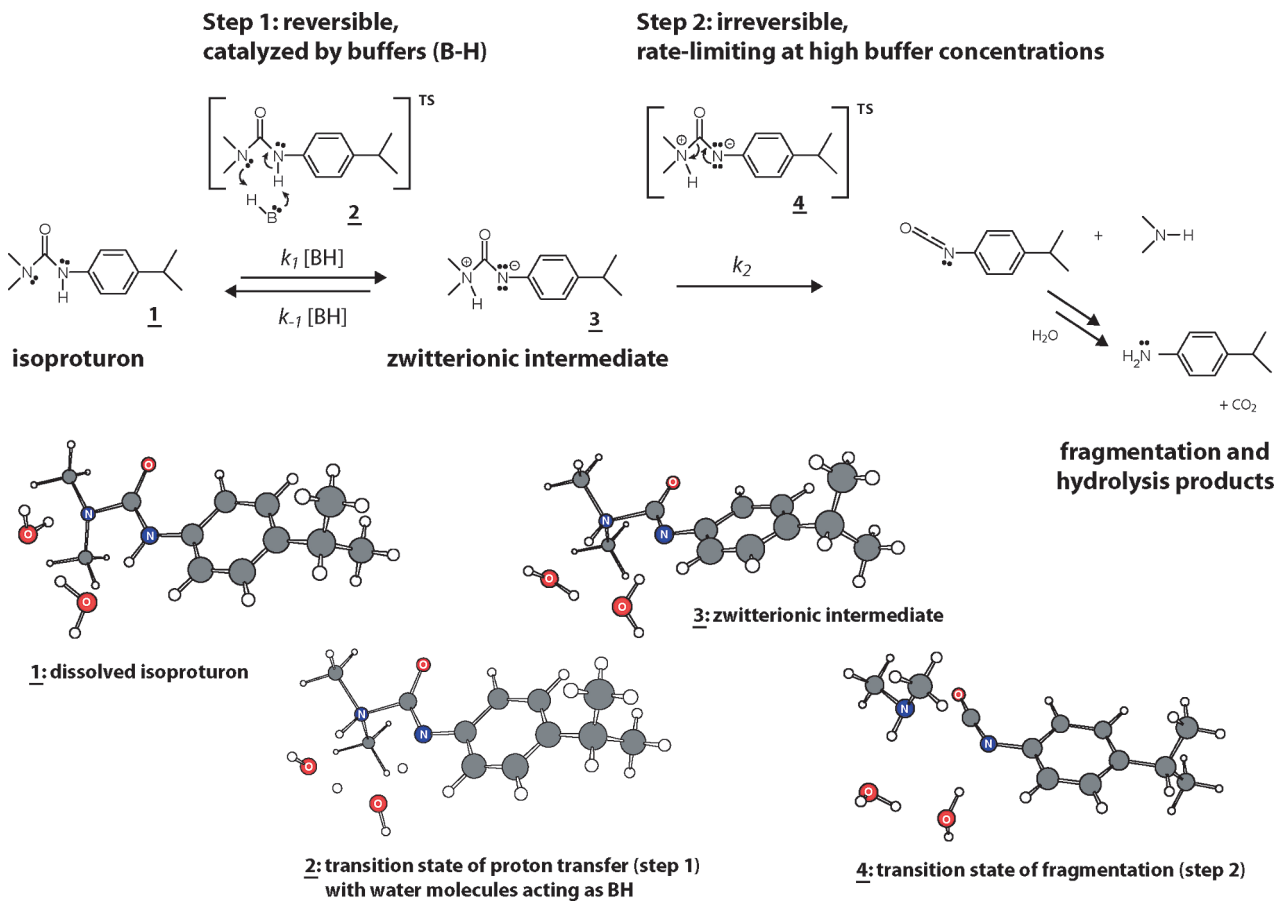

FIGURE 1. Reaction scheme of the postulated mechanism for hydrolysis of isoproturon at 60 °C (*16*), together with our computed structures of disolvated minima (1 and 3) and TS structures (2 and 4) optimized at the *m*PWPW91/6−31+G(d,p) level.

two defined fragments so that isotope ratios are not only determined as an average over the whole compound, but also in separate parts of the molecule (Scheme 1).

Here, the dimethylamine fragment (DMA) reflects the isotopic changes at the alkyl nitrogen atom and the two adjacent methyl carbon atoms of unreacted isoproturon, whereas the isocyanate fragment (ISO) preserves isotopic shifts at the aryl nitrogen atom and the rest of the carbon atoms. By analyzing the two fragments separately, it is therefore possible to determine fragment-, or even position-specific isotope effects in isoproturon; these give enhanced mechanistic insight. On the other hand, average ("bulk") isotopic ratios may be reconstructed giving the information that would be commonly measured with conventional GC-IRMS.

The particular objectives of this study were as follows:

(1) To investigate to which extent variations of experimental parameters influencing the hydrolysis rate (e.g., buffer or pH) may change observable isotope fractionation at certain molecular positions.

(2) To mathematically rationalize the relationship between rate constants and isotope fractionation based on theoretical considerations.

(3) To evaluate how the experimentally determined isotope fractionation at specific molecular positions agrees with the hypothesized mechanism of the two-step reaction and with calculated equilibrium isotope effects for the first reaction step.

(4) To evaluate, based on the isotope enrichment factors and dual isotope slopes determined in this study, under which circumstances CSIA can be applied to identify and quantify natural multistep reactions.

Experimental Section

Chemicals. Isoproturon (3-(4-isopropylphenyl)-1,1-dimethylurea; CAS 34123−59−6) was from Tropitzsch (>98%; Marktredwitz, Germany); for further chemicals see the Supporting Information (SI).

Isotope and Quantitative Analysis. Purified isoproturon was analyzed on a GC-C-IRMS system (Thermo Fisher Scientific) with the method described by Penning and Elsner (*21*). Briefly, injected isoproturon was dried in an Optic 3 temperature-programmable high-performance injector (ATAS GL International B.V., Veldhoven, The Netherlands) at 20 °C and then transferred at 400 °C to a DB-624 column (60 m × 0.25 mm; 1.4 μm film; J&W Scientific) operated at 240 °C. At these high temperatures, isoproturon fragmented into dimethylamine (DMA) and 4-isopropylphenylisocyanate (ISO) (see Scheme 1). The fragments were separated on the GC column and individually analyzed by IRMS. This method allows determination of isotope ratios in each nitrogen position as well as for the average of the two methyl carbon atoms in DMA. In addition, the weighted isotopic average of the remaining 10 carbon atoms in ISO is determined.

The δ^{15}N-and δ^{13}C-values are reported in per mil relative to Vienna PeeDee Belemnite (VPDB) and air respectively:

$$\delta^{13}C = [(^{13}C/^{12}C_{sample} - {}^{13}C/^{12}C_{standard})/{}^{13}C/^{12}C_{standard}] \times 1000$$

$$\delta^{15}N = [(^{15}N/^{14}N_{sample} - {}^{15}N/^{14}N_{standard})/{}^{15}N/^{14}N_{standard}] \times 1000$$

CO_2 and N_2 reference gas were calibrated to V-PDB and air, respectively, as described in ref *21*.

Concentrations of isoproturon and its degradation products were analyzed by reverse-phase chromatography with UV detection at 240 nm (*21*).

SCHEME 1

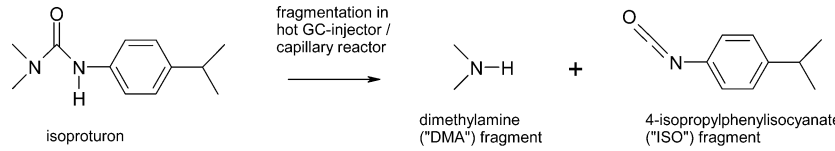

Hydrolysis Experiments. Triplicate hydrolysis experiments (250−300 mL) of 22 mg L^{-1} isoproturon were conducted at 60 °C. pH was varied using 50 mM phosphate buffer at pH 3.3, 4.2, 6.2, 7.2, 8.4, 12.0, and 50 mM borate buffer at pH 10.3. To systematically vary ionic strength, experiments were conducted (i) in Millipore water at pH 5.4; (ii) with 1 M KCl at pH 5.3 (I = 1 M); (iii) with 0.3 M phosphate buffer and 0.4 KCl at pH 6.6 (I = 1 M); (iv) with 0.3 M phosphate buffer at pH 6.5 (I = 0.6 M). At each sampling event, 300 μL samples were taken for quantification and 20−80 mL was taken for isotope analysis. The latter samples were extracted with 5 or 10 mL of dichloromethane and dried completely at room temperature under the hood to evaporate 4-isopropylaniline (hydrolysis product). Complete removal of 4-isopropylaniline was confirmed by HPLC. Tests with standards and also the initial samples of the hydrolysis experiment showed that this purification by evaporation did not significantly change (<0.3‰ for carbon and <0.5‰ for nitrogen) the isotope composition of isoproturon. Purified and dried extracts were redissolved in dichloromethane giving a final concentration of approximately 500 mg L^{-1}. From these solutions, 2 and 9 μL aliquots were injected for carbon and nitrogen isotope analysis, respectively.

Determination of ϵ According to the Rayleigh Equation.

$$\ln\left(\frac{1000+\delta^h E_t}{1000+\delta^h E_0}\right)=\frac{\varepsilon}{1000}\ln f \tag{1}$$

The linearized Rayleigh equation (eq 1) was applied to derive fragment-specific isotopic enrichment factors ϵ_{DMA} and ϵ_{ISO} reported in per mil (‰) where f is the fraction of compound that has not yet reacted, and $\delta^h E_t$ and $\delta^h E_0$ are the isotopic signatures of a given fragment for the element E at times t and zero, respectively. If ε is position-specific, as it is with nitrogen in each fragment, an apparent kinetic isotope effect (AKIE) can be calculated as

$$\mathrm{AKIE}=\left(\frac{\varepsilon}{1000}+1\right)^{-1} \tag{2}$$

The same formula applies to calculate the average secondary isotope effect of the two carbon atoms of DMA, which are equivalent in the fragment, but not in isoproturon. In contrast, the AKIE at the reacting carbonyl atom is "diluted" in the average bulk ϵ of the ISO fragment (10 carbon atoms, of which nine are nonreactive) so that (*5*)

$$A\mathrm{KIE}_{\mathrm{carbonyl}}\approx\left(\frac{10\cdot\varepsilon_{\mathrm{ISO,carbon}}}{1000}+1\right)^{-1} \tag{3}$$

Finally, conventional bulk isotopic enrichment factors ϵ_{bulk} may be calculated from the weighted average of the fragment-specific factors ε_{DMA} and ε_{ISO} according to

$$\varepsilon_{\mathrm{bulk,nitrogen}}=\frac{\varepsilon_{\mathrm{DMA,nitrogen}}+\varepsilon_{\mathrm{ISO,nitrogen}}}{2} \tag{4}$$

and

$$\varepsilon_{\mathrm{bulk,carbon}}=\frac{2\cdot\varepsilon_{\mathrm{DMA,carbon}}+10\cdot\varepsilon_{\mathrm{ISO,carbon}}}{12} \tag{5}$$

Computational Methods. To model the equilibrium isotope effect of the hydrolysis reaction, two supermolecular structures were considered, namely, the normal and zwitterionic tautomers of isoproturon, each complexed by two water molecules (Figure 1). The geometries of these structures were fully optimized at the density functional level of theory using the generalized gradient approximation functional *m*PWPW91 (*22*−*24*), the 6−31+G(d,p) basis set (*25*) on all atoms, and an automatically generated auxiliary basis set for use in Coulomb integral calculations making use of the resolution of the identity approximation. Analytic vibrational frequency calculations were performed to verify that the final structures were local minima and to compute thermal contributions to the 333.15 K (60 °C) free energy using the ideal-gas, rigid-rotator, harmonic-oscillator approximation (*26*). These free energies were computed for all relevant C and N isotopic substitutions and variations therein were used to compute in the usual fashion (*26*) the equilibrium isotope effect (EIE) between isoproturon and its zwitterionic tautomer.

In addition, transition-state (TS) structures were computed for the water-assisted proton-transfer reaction connecting the two tautomers of isoproturon and for the dissociation of the zwitterion (Figure 1). We consider these structures because they provide some insight into the relative energetics of the two reaction steps. However, while complexation with two water molecules mimics some of the effects of bulk solvation, we expect there to be a systematic bias against zwitterionic species because we ignore remaining solute−solvent interactions. While including such interactions via a continuum solvation model seems like an obvious choice (*27*), we found that numerical noise associated with the relevant self-consistent reaction field equations made it impossible to optimize structures sufficiently tightly to deliver well converged vibrational frequencies (and hence isotope effects). Because the TS structures, with their partially formed bonds, are much more sensitive to any failure to fully account for aqueous solvation, we do not attempt to compute KIEs directly, but given the stiffer nature of minimum-energy structures we consider our supermolecular EIE calculations to be more reliable.

All calculations were performed with the Gaussian 03 suite of electronic structure programs (*28*).

Results and Discussion

Variation of Isotope Fractionation Depending on Experimental Conditions during Hydrolysis of Isoproturon. Influence on isotope fractionation was tested at different pH and different buffer concentrations. Under all conditions, hydrolysis rates were pseudofirst order with respect to isoproturon (SI Figure S-1) and the experimental k_{obs} varied within one order of magnitude (Table 1), consistent with previous findings (*16*). Table 1 and Figure 2 show that heavy isotopes became enriched in both fragments and for both elements, carbon and nitrogen, but that this enrichment depended strongly on reaction conditions and was fragment-specific. In particular, panels a and b in Figure 2 demonstrate that nitrogen enrichment factors ε were largely constant in the aryl nitrogen (ISO fragment), but highly variable in the alkyl nitrogen (DMA fragment). As shown in Table 1, variation was also encountered for carbon enrichment factors in both fragments, as well as for average $\varepsilon_{bulk,\ carbon}$ and $\varepsilon_{bulk,\ nitrogen}$

TABLE 1. Rate Constants and Isotope Enrichment Factors of All Experiments, Together with Measured and Calculated Isotope Effects

pH	buffer/salt	k_{obs} 10^7 (s^{-1})	$\varepsilon_{DMA\ carbon}$ [‰]	$\varepsilon_{ISO\ carbon}$ [‰]	$\varepsilon_{bulk\ carbon}$ [‰]	$\varepsilon_{DMA\ nitrogen}$ [‰]	$\varepsilon_{ISO\ nitrogen}$ [‰]	$\varepsilon_{bulk\ nitrogen}$ [‰]	$(\varepsilon N/\varepsilon C)_{DMA}$	$(\varepsilon N/\varepsilon C)_{ISO}$	$(\varepsilon N/\varepsilon C)_{bulk}$
12.0	0.05 M phosphate	33.2 ± 1.0	−2.5 ± 0.2	−4.5 ± 0.1	−4.2 ± 0.1	−19.9 ± 0.5	−10.7 ± 0.3	−15.3 ± 0.6	8.0 ± 0.7	2.4 ± 0.1	3.7 ± 0.2
6.6	0.3 M phosphate, 0.4 M KCl	24.8 ± 0.1	−2.7 ± 0.3	−4.5 ± 0.2	−4.2 ± 0.2	−18.0 ± 0.9	−10.2 ± 0.3	−14.1 ± 0.9	6.7 ± 0.8	2.3 ± 0.1	3.4 ± 0.3
6.5	0.3 M phosphate	24.5 ± 0.3	−2.8 ± 0.1	−4.2 ± 0.1	−4.0 ± 0.1	−20.8 ± 1.1	−9.3 ± 0.1	−15.1 ± 1.1	7.4 ± 0.5	2.2 ± 0.0	3.8 ± 0.3
6.2	0.05 M phosphate	20.0 ± 1.1	−1.9 ± 0.1	−3.5 ± 0.1	−3.2 ± 0.1	−12.2 ± 0.4	−9.3 ± 0.3	−10.8 ± 0.5	6.4 ± 0.4	2.7 ± 0.1	3.3 ± 0.2
4.2	0.05 M phosphate	19.0 ± 0.8	−1.8 ± 0.2	−3.5 ± 0.1	−3.2 ± 0.1	−12.9 ± 0.3	−9.0 ± 0.2	−11.0 ± 0.4	7.2 ± 0.8	2.6 ± 0.1	3.4 ± 0.2
10.3	0.05 M borate	17.8 ± 0.9	−1.4 ± 0.1	−3.3 ± 0.2	−3.0 ± 0.2	−9.4 ± 0.2	−10.2 ± 0.1	−9.8 ± 0.2	6.7 ± 0.5	3.1 ± 0.2	3.3 ± 0.2
3.3	0.05 M phosphate	17.2 ± 0.7	−2.3 ± 0.1	−3.7 ± 0.2	−3.5 ± 0.2	−16.3 ± 0.6	−9.2 ± 0.3	−12.8 ± 0.7	7.1 ± 0.4	2.5 ± 0.2	3.7 ± 0.3
7.2	0.05 M phosphate	15.3 ± 0.6	−1.4 ± 0.1	−3.2 ± 0.1	−2.9 ± 0.1	−9.8 ± 0.5	−8.4 ± 0.7	−9.1 ± 0.9	7.0 ± 0.6	2.6 ± 0.2	3.1 ± 0.3
8.4	0.05 M phosphate	8.8 ± 0.4	−1.2 ± 0.2	−3.0 ± 0.1	−2.7 ± 0.1	−7.7 ± 0.3	−10.2 ± 0.4	−9.0 ± 0.5	6.4 ± 1.1	3.4 ± 0.2	3.3 ± 0.2
5.3	1 M KCl	6.3 ± 0.1	−1.8 ± 0.1	−2.3 ± 0.1	−2.2 ± 0.1	−5.6 ± 0.2	−7.5 ± 0.6	−6.6 ± 0.6	3.1 ± 0.2	3.3 ± 0.3	3.0 ± 0.3
5.4	none	3.1 ± 0.1	−1.4 ± 0.3	−2.4 ± 0.1	−2.2 ± 0.1	−4.9 ± 0.7	−8.8 ± 0.3	−6.9 ± 0.8	3.5 ± 0.9	3.7 ± 0.2	3.1 ± 0.4

step 1	DMA carbon	ISO carbon	bulk carbon	alkyl nitrogen	aryl nitrogen	bulk nitrogen	$(\varepsilon N/\varepsilon C)_{DMA}$	$(\varepsilon N/\varepsilon C)_{ISO}$	$(\varepsilon N/\varepsilon C)_{bulk}$
ε for step 1 being rate-determining (intercept of regression k_{obs} vs ε)	−1.1‰ ± 0.3‰	−2.1‰ ± 0.2‰	−1.9‰ ± 0.2‰	−2.5‰ ± 1.7‰	−8.2‰ ± 0.5‰	−5.4‰ ± 0.9‰	2.3 ± 1.6	4.0 ± 0.4	2.8 ± 0.5
KIE_1 (derived from ε of step 1 being rate-determining)	1.001 ± 0.0003[a]	1.021 ± 0.002[b]		1.002 ± 0.002[a]	1.008 ± 0.001[a]				
$EIE_{1\text{-cal}}$ from computational calculations	1.001/0.998	1.016		0.992	1.013				

step 2	DMA carbon	ISO carbon	bulk carbon	alkyl nitrogen	aryl nitrogen	bulk nitrogen	$(\varepsilon N/\varepsilon C)_{DMA}$	$(\varepsilon N/\varepsilon C)_{ISO}$	$(\varepsilon N/\varepsilon C)_{bulk}$
ε for step 2 being rate-determining (approximated by value at pH 12)	−2.5‰ ± 0.2‰	−4.5‰ ± 0.1‰	−4.2‰ ± 0.1‰	−19.9‰ ± 0.5‰	−10.7‰ ± 0.3‰	−15.3‰ ± 0.6‰	8.0 ± 0.7	2.4 ± 0.1	3.7 ± 0.2
$EIE_1 \cdot KIE_2$ (derived from ε of experiment at pH 12)	1.003 ± 0.0002[a]	1.047 ± 0.001[b]		1.020 ± 0.001[a]	1.011 ± 0.0003[a]				
KIE_2 (estimated as experimental $EIE_1 \cdot KIE_2$ divided by $EIE_{1\text{-cal}}$)	1.003	1.031		1.029	0.998				

[a] Calculated according to eq 2. [b] Calculated according to eq 3.

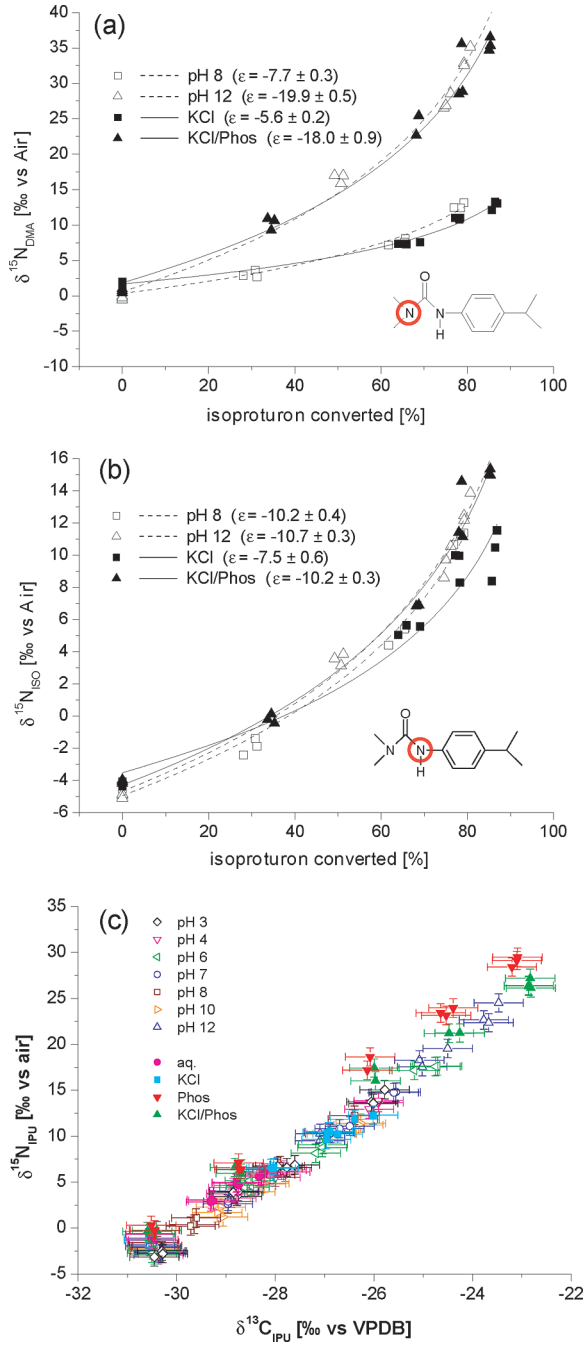

FIGURE 2. Nitrogen isotope enrichment at (a) the alkyl N position and (b) the aryl N position of unreacted isoproturon for four different reaction conditions spanning the range of observed isotope enrichment factors. Regression lines are fits according to the Rayleigh equation (eq 1) and calculated ε values are given. (c) Dual isotope plot of bulk isotope ratios $\delta^{15}N_{bulk}$ versus $\delta^{13}C_{bulk}$ derived analogous to eqs 4 and 5.

values. On the other hand, when plotting molecular average isotope ratios $\delta^{15}N_{bulk}$ and $\delta^{13}C_{bulk}$ in a dual isotope plot, Figure 2c shows that a remarkably consistent slope was obtained for all experiments, which may potentially be used to identify the reaction in unknown systems, similar to that known from previous applications (*2*−*5*).

Mathematical Derivation of the Correlation of AKIE with k_{obs}. Even though the changes in bulk isotope ratios show similar trends as known from earlier studies - variable ϵ-values, consistent dual isotope slopes - our fragment-specific information indicates that the underlying mechanism is likely more complicated. A fundamental understanding is desirable. The following mathematical treatment therefore attempts to link the observable isotope fractionation to reaction rates.

The reaction of Figure 1 may be described by the following scheme:

$$S \underset{k_{-1}[BH]}{\overset{k_1[BH]}{\rightleftarrows}} I \xrightarrow{k_2} P \tag{6}$$

where *S* is the substrate isoproturon, BH is the buffer, I is the zwitterionic intermediate, P is the product, and the various *k* are elementary rate constants for the respective reaction steps. Derived steady state treatments shown in the Supporting Information describe the influence of buffer concentration [BH] on the reaction rate k_{obs}

$$k_{obs} = \frac{k_2 k_1 [BH]}{k_2 + k_{-1}[BH]} \tag{7}$$

as well as on the apparent kinetic isotope effect AKIE

$$AKIE = \frac{EIE_1KIE_2 + KIE_1\dfrac{k_2}{k_{-1}[BH]}}{1 + \dfrac{k_2}{k_{-1}[BH]}} \tag{8}$$

Here, $KIE_1 = {}^{l}k_1/{}^{h}k_1$, $KIE_2 = {}^{l}k_2/{}^{h}k_2$, and $EIE_1 = ({}^{l}k_1/{}^{h}k_1)/({}^{l}k_{-1}/{}^{h}k_{-1})$ are the position-specific kinetic and equilibrium isotope effects of the respective reaction steps, with superscripts "l" and "h" denoting light and heavy isotopes at the reactive position; AKIEs are linked to the enrichment factors of the Rayleigh equation according to eqs 2 and 3 (*5*). [BH] may be interpreted as an effective buffer concentration which weighs the buffer concentration by its effectiveness in catalyzing the reaction. With this meaning of [BH], eqs 7 and 8 are applicable to different kinds of chemical species.

From eq 8, maximum and minimum AKIE values can be predicted. Specifically, AKIE vary between KIE_1 for very small concentrations of BH and EIE_1KIE_2 for very large concentrations of BH:

$$AKIE_{BH\to 0} = KIE_1 \tag{9}$$

$$AKIE_{BH\to\infty} = EIE_1KIE_2 \tag{10}$$

Likewise, k_{obs} values of eq 7 vary between a theoretical value of zero in the absence of any buffer—a situation unlikely to be encountered experimentally, since water molecules are always present as weak buffers—and a maximum value for large concentrations of BH:

$$k_{obs}([BH]_{BH\to 0}) = 0 \tag{11}$$

$$k_{obs}([BH]_{BH\to\infty}) = k_1\frac{k_2}{k_{-1}} = k_{obs,max} \tag{12}$$

In order to combine eqs 7 and 8, we rearrange eq 7

$$k_{obs} = \frac{k_2k_1[BH]}{k_2 + k_{-1}[BH]} = \frac{\dfrac{k_2k_1[BH]}{k_{-1}[BH]}}{\dfrac{k_2}{k_{-1}[BH]} + 1} = \frac{\dfrac{k_2k_1}{k_{-1}}}{1 + \dfrac{k_2}{k_{-1}[BH]}} = \frac{k_{obs,max}}{1 + \dfrac{k_2}{k_{-1}[BH]}} \tag{13}$$

leading to

$$\frac{1}{1 + \dfrac{k_2}{k_{-1}[BH]}} = \frac{k_{obs}}{k_{obs,max}} \tag{14}$$

and

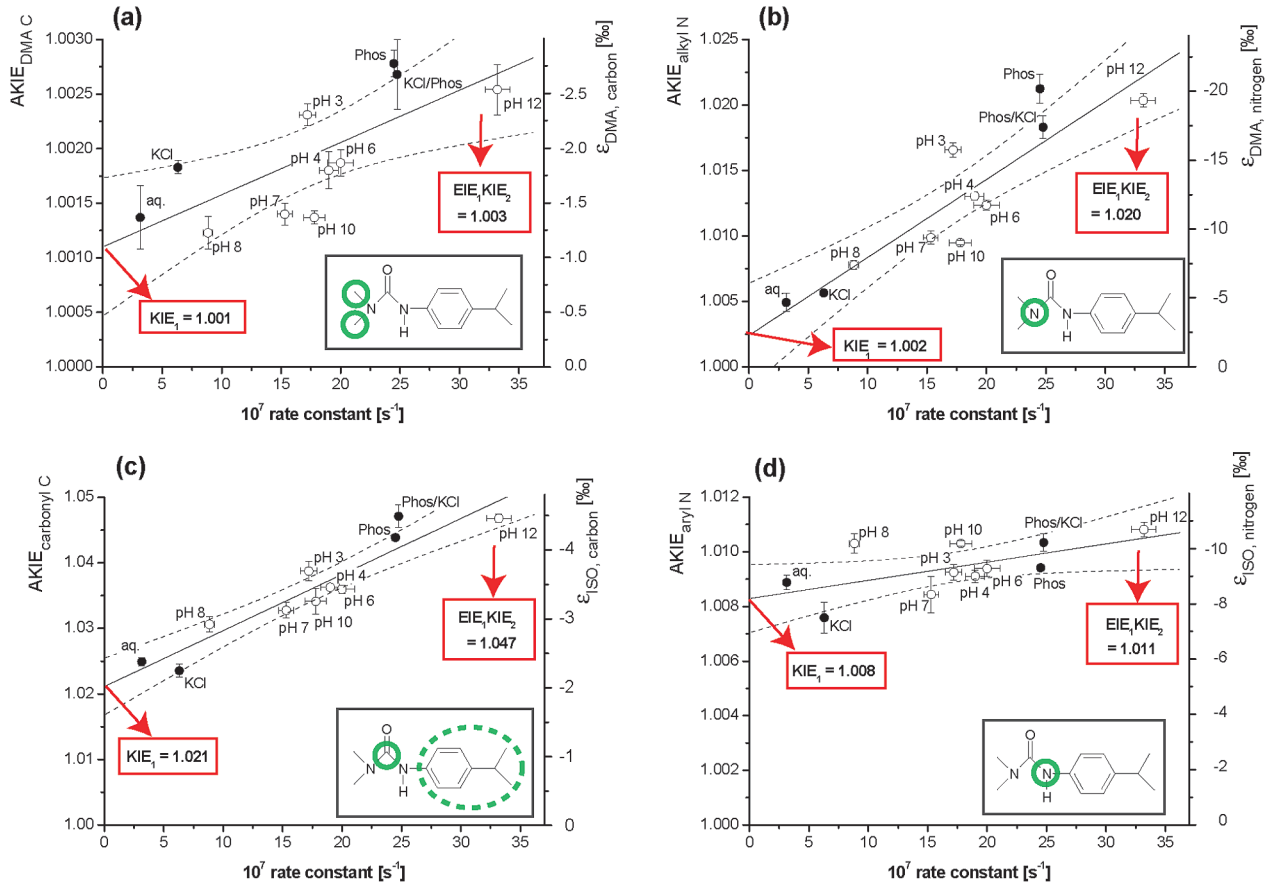

FIGURE 3. Correlation of observable isotope fractionation with reaction rates k_{obs} for different molecular parts of isoproturon: (a) the methyl carbons of the DMA group, (b) the alkyl nitrogen, (c) the carbonyl carbon, and (d) the aryl nitrogen. Enrichment factors ε given on the right-hand axis were converted to AKIE values given on the left-hand axis according to eq 2 (panels a, b, and d) and eq 3 (panel c). Experiments with constant buffer concentration and changing pH are shown as open symbols and labeled with their pH value. Other experiments shown in closed symbols are labeled by a combination of phosphate buffer and KCl (aq.: in aqueous solution; KCl: in 1 M KCl; Phos: in 0.3 M phosphate buffer; Phos/KCl: in 0.3 M phosphate and 0.4 M KCl). Error bars are the standard deviation of k_{obs} and KIE from triplicate experiments, and dashed lines represent 95% confidence intervals of the regression. Based on eq (*16*), a linear regression was employed to relate KIE and k_{obs}. The Figure illustrates that KIE_1 values were determined from the regression line intercept and the product EIE_1KIE_2 was obtained from values at pH 12, where previous studies have shown that $k_{obs,max}$ is at a maximum (*16*).

$$\frac{\dfrac{k_2}{k_{-1}[BH]}}{1+\dfrac{k_2}{k_{-1}[BH]}} = \left(1-\frac{k_{obs}}{k_{obs,max}}\right) \qquad (15)$$

Substitution into eq 8 gives

$$AKIE = \frac{k_{obs}}{k_{obs,max}} \cdot EIE_1KIE_2 + \left(1-\frac{k_{obs}}{k_{obs,max}}\right) \cdot KIE_1$$
$$= KIE_1 + \frac{k_{obs}}{k_{obs,max}} \cdot (EIE_1KIE_2 - KIE_1) \qquad (16)$$

Therefore, kinetic isotope fractionation in the abiotic hydrolysis of isoproturon is expected to vary linearly with observable reaction rates. This is in stark contrast to most environmental reactions where no rate-dependence is observed. Equation 16 also allows extracting the maximum and minimum values for AKIE and ϵ values from experimental data. While KIE_1, the kinetic isotope effect of the first step, may be obtained as intercept of a linear regression, EIE_1KIE_2 can be determined from AKIE values at $k_{obs,max}$. In our case, this corresponds to the experiment at pH 12 where previous studies have shown that maximum reaction rates were reached (*16*).

Linear Regression of AKIE vs k_{obs}. Figure 3 shows that experimentally measured isotope fractionation did indeed vary linearly with reaction rates, as predicted by eq 16. Deviations are likely attributable to subtle differences in transition state structure considering that different chemical buffer species were involved. The overall good correlation, however, confirms the mechanistic model and demonstrates that essentially the same reaction mechanism prevailed in the different experiments. Figure 3 also illustrates how values of KIE_1 and EIE_1KIE_2 may successfully be evaluated from the regression. These numbers are summarized again in Table 1.

Comparison of Experimentally Determined Isotope Effects with the Hypothesized Reaction Mechanism and Calculated Isotope Effects. To understand the mechanistic reason for observed changes in fractionation, the isotope effects KIE_1 and EIE_1KIE_2 from the linear regression may be compared to expectations from theory. Table 1 lists equilibrium isotope effects $EIE_{1\text{-cal}}$ calculated for the first reaction step based on computational modeling of disolvated isoproturon and the disolvated zwitterion (see the Computational Methods section).

First Reaction Step. For the aryl nitrogen, both our experimental KIE_1 of 1.008 ± 0.0006 as well as the $EIE_{1\text{-cal}}$ = 1.013 are consistent with NH bond breakage in the first step. At the carbonyl carbon, substantial values of KIE_1 = 1.021 ± 0.0006 and $EIE_{1\text{-cal}}$ = 1.016 agree with the prediction that the C—N bond is considerably lengthened in the zwitterion (1.61 Å). For the methyl carbons, isotope effects KIE_1 and

$EIE_{1\text{-cal}}$ are, as expected, of secondary nature. At the alkyl nitrogen, finally, an inverse $EIE_{1\text{-cal}}$ of 0.992 is calculated. This reflects the fact that the atom undergoes hybridization from sp^2 to sp^3 during protonation leading to more constrained molecular vibrations in the zwitterion. The experimental observation of a normal (i.e., larger than unity) kinetic isotope effect of $KIE_1 = 1.003 \pm 0.002$ at this position may indicate that deprotonation and reprotonation are not concerted in the fully solvated system, and that the former is rate determining so that the inverse effect is not fully expressed. In general, however, KIE_1 and $EIE_{1\text{-cal}}$ are remarkably consistent with respect to trends and magnitude in all positions. This likely reflects the fact that the zwitterion formation is highly endergonic so that the transition state is late and resembles to a considerable extent the zwitterionic intermediate.

Second Step. Calculated $EIE_{1\text{-cal}}$ may also be used to estimate KIE_2 values of the second reaction step according to

$$KIE_{2,\text{estimate}} = \frac{(EIE_1 \cdot KIE_2)_{\text{experimental}}}{EIE_{1\text{-cal}}} \tag{17}$$

The summarized results in Table 1 show that pronounced KIE_2 are only encountered at the alkyl nitrogen and the carbonyl carbon. Since these are the positions where a C—N bond is broken in this step, the result is again in full agreement with the mechanistic hypothesis.

Energetics. Considering the relative energetics of the two initial reaction steps, our density functional (DFT) calculations predict free energies of activation of 13.5 and 17.7 kcal mol^{-1}, respectively (both relative to the starting isoproturon). We note, however, that the second value may be too high. The second TS structure is substantially more zwitterionic, and we would indeed expect structures with increasing zwitterionic character to be increasingly overestimated in energy. The reason is incomplete solvation using a microsolvated cluster without continuing additional solvation (see Computational Methods). In addition, there may be variations associated with the action of proton shuttle mediators other than the two water molecules considered here that would bring the two transition states to near degeneracy. Our DFT results are therefore consistent with the experimental observation that either step may be rate determining.

Significance for the Application of CSIA to Identify and Quantify Natural Multistep reactions. The mechanistic understanding now makes it possible to appreciate the factors that are responsible for the observed changes in apparent isotope fractionation. If kinetic and equilibrium isotope effects of the first step are similarly expressed, as suggested by our data ($KIE_1 \approx EIE_{1\text{-cal}}$), Equation 16 simplifies to

$$\begin{aligned} AKIE &= KIE_1 + \frac{k_{obs}}{k_{obs,max}} \cdot (EIE_1 KIE_2 - KIE_1) \\ &\approx KIE_1 + \frac{k_{obs}}{k_{obs,max}} \cdot (KIE_1 KIE_2 - KIE_1) \\ &= KIE_1 \left(1 + \frac{k_{obs}}{k_{obs,max}} \cdot (KIE_2 - 1)\right) \end{aligned} \tag{18}$$

meaning that the variation in AKIE is primarily attributable to the second step. Indeed, large variations in ϵ are observed specifically at the alkyl N position where the KIE_1 is near unity and the KIE_2 is large. In contrast, only small variations are observed at the aryl N position, where the KIE_1 is large and the KIE_2 is close to unity (Figure 2 and 3). If fragment-specific isotope ratios can be measured, $\epsilon_{\text{ISO nitrogen}}$ may therefore be taken as a reasonably robust parameter to quantify the extent of transformation for the mechanism, irrespective of which step is rate-limiting (see Table 1). In contrast, Table 1 demonstrates that if only $\epsilon_{\text{bulk nitrogen}}$ values are available, such estimates would be associated with a greater uncertainty.

Our results also suggest that the remarkably consistent slope of $\delta^{15}N_{bulk}/\delta^{13}C_{bulk} = \varepsilon_{N,\text{ bulk}}/\varepsilon_{C,\text{ bulk}}$ in Figure 2c is formed serendipitously. As shown in Table 1, the corresponding slopes of the respective fragments $\varepsilon_{N,\text{ ISO}}/\varepsilon_{C,ISO}$, and $\epsilon_{N,DMU}/\epsilon_{C,DMA}$, are not constant, but vary significantly depending on reaction conditions. Because the trends are counter to each other, however, they largely compensate in their average so that overall a consistent slope is obtained. In other words, the aryl nitrogen position shows isotope fractionation mostly in the first and the alkyl nitrogen position mostly in the second step; by coincidence, their average happens to vary in the same way as the average of the carbon isotope effects.

Considering more general cases of other compounds and other transformation reactions, our insight from this study therefore suggests that more complicated scenarios may be encountered than commonly expected. For once, isotope fractionation in simple chemical multistep reactions can respond to subtle changes in reaction conditions in a remarkably sensitive way. Adding 50 mM phosphate buffer at pH 6 more than doubled the nitrogen isotopic enrichment factor at the alkyl position of isoproturon from -4.9 ± 0.7‰ to -12.2 ± 0.4‰ (see Table 1). Second, isotope fractionation under such conditions may directly correlate with observable reaction rates, which is seldom observed. Similarly as known from earlier studies, this variability makes it difficult to choose ϵ values to quantify the extent of transformation (*2, 29*). Unlike previous investigations, however, we found that also slopes in dual isotope plots can be variable. Care must be taken that such differences are not interpreted as indication of a second, parallel degradation pathway when instead the same transformation mechanism prevails, but only a different step becomes rate-limiting.

Finally our study shows that intramolecular isotope analysis of molecular fragments may be a way to circumvent these problems. With fragment specific resolution, it can become possible to identify robust ϵ values and consistent dual isotope slopes in certain molecular positions that allow conventional applications of CSIA. The simultaneous determination of position-specific isotope effects may create the complementary mechanistic understanding that puts such approaches on a sound scientific basis. In our case, we identified $\delta^{15}N_{bulk}/\delta^{13}C_{bulk} = \varepsilon_{N,\text{ bulk}}/\varepsilon_{C,\text{ bulk}}$ as a consistent slope that holds promise to detect the zwitterionic mechanism of isoproturon hydrolysis in unknown systems, and the enrichment factor $\varepsilon_{\text{ISO nitrogen}}$ as a robust parameter to quantify this extent of transformation. Future work will investigate how these patterns compare to isotope fractionation of isoproturon in biotransformation reactions.

Acknowledgments

This work was conducted in a Helmholtz Young Investigator Group supported by funding of the Helmholtz Initiative and Networking Fund. CJC thanks the U.S. National Science Foundation for support (CHE06−10183).

Supporting Information Available

Additional information as noted in text. This material is available free of charge via the Internet at http://pubs.acs.org.

Literature Cited

(1) Schmidt, T. C.; Zwank, L.; Elsner, M.; Berg, M.; Meckenstock, R. U.; Haderlein, S. B. Compound-specific stable isotope analysis of organic contaminants in natural environments: A critical review of the state of the art, prospects, and future challenges. *Anal. Bioanal. Chem.* **2004**, *378*, 283–300.

(2) Elsner, M.; McKelvie, J.; LacrampeCouloume, G.; SherwoodLollar, B. Insight into methyl tert-butyl ether (MTBE) Stable isotope fractionation from abiotic reference experiments. *Environ. Sci. Technol.* **2007**, *41*, 5693–5700.

(3) Zwank, L.; Berg, M.; Elsner, M.; Schmidt, T. C.; Schwarzenbach, R. P.; Haderlein, S. B. New evaluation scheme for two-dimensional isotope analysis to decipher biodegradation processes: Application to groundwater contamination by MTBE. *Environ. Sci. Technol.* **2005**, *39*, 1018–1029.
(4) Kuder, T.; Wilson, J. T.; Kaiser, P.; Kolhatkar, R.; Philp, P.; Allen, J. Enrichment of stable carbon and hydrogen isotopes during anaerobic biodegradation of MTBE: Microcosm and field evidence. *Environ. Sci. Technol.* **2005**, *39*, 213–220.
(5) Elsner, M.; Zwank, L.; Hunkeler, D.; Schwarzenbach, R. P. A new concept linking observable stable isotope fractionation to transformation pathways of organic pollutants. *Environ. Sci. Technol.* **2005**, *39*, 6896–6916.
(6) Sherwood Lollar, B.; Slater, G. F.; Sleep, B.; Witt, M.; Klecka, G. M.; Harkness, M.; Spivack, J. Stable carbon isotope evidence for intrinsic bioremediation of tetrachloroethene and trichloroethene at Area 6, Dover Air Force Base. *Environ. Sci. Technol.* **2001**, *35*, 261–269.
(7) Meckenstock, R. U.; Morasch, B.; Griebler, C.; Richnow, H. H. Stable isotope fractionation analysis as a tool to monitor biodegradation in contaminated acquifers. *J. Contam. Hydrol.* **2004**, *75*, 215–255.
(8) Fischer, A.; Bauer, J.; Meckenstock, R. U.; Stichler, W.; Griebler, C.; Maloszewski, P.; Kastner, M.; Richnow, H. H. A multitracer test proving the reliability of Rayleigh equation-based approach for assessing biodegradation in a BTEX contaminated aquifer. *Environ. Sci. Technol.* **2006**, *40*, 4245–4252.
(9) Mancini, S. A.; Hirschorn, S. K.; Elsner, M.; Lacrampe-Couloume, G.; Sleep, B. E.; Edwards, E. A.; SherwoodLollar, B. Effects of trace element concentration on enzyme controlled stable isotope fractionation during aerobic biodegradation of toluene. *Environ. Sci. Technol.* **2006**, *40*, 7675–7681.
(10) Penning, H.; Plugge, C. M.; Galand, P. E.; Conrad, R. Variation of carbon isotope fractionation in hydrogenotrophic methanogenic microbial cultures and environmental samples at different energy status. *Global Change Biol.* **2005**, *11*, 2103–2113.
(11) Nijenhuis, I.; ert, J.; Beck, K.; Kastner, M.; Diekert, G.; Richnow, H. H. Stable isotope fractionation of tetrachloroethene during reductive dechlorination by *Sulfurospirillum multivorans* and *Desulfitobacterium* sp. strain PCE-S and abiotic reactions with cyanocobalamin. *Appl. Environ. Microbiol.* **2005**, *71*, 3413–3419.
(12) Cichocka, D.; Imfeld, G.; Richnow, H.-H.; Nijenhuis, I. Variability in microbial carbon isotope fractionation of tetra- and trichloroethene upon reductive dechlorination. *Chemosphere* **2008**, *71*, 639–648.
(13) Northrop, D. B. Steady-state analysis of kinetic isotope effects in enzymatic reactions. *Biochemistry* **1975**, *14*, 2644–2651.
(14) Fischer, A.; Theuerkorn, K.; Stelzer, N.; Gehre, M.; Thullner, M.; Richnow, H. H. Applicability of stable isotope fractionation analysis for the characterization of benzene Biodegradation in a BTEX-contaminated aquifer. *Environ. Sci. Technol.* **2007**, *41*, 3689–3696.
(15) Giffney, C. J.; O'Connor, C. J. Hydrolysis of phenylureas. Part II. Hydrolysis in acid and aqueous solutions. *J. Chem. Soc., Perkin Trans. 2* **1976**, *36*, 2–368.
(16) Salvestrini, S.; Di Cerbo, P.; Capasso, S. Kinetics and mechanism of hydrolysis of phenylureas. *J. Chem. Soc., Perkin Trans. 2* **2002**, 1889–1893.
(17) Laudien, R.; Mitzner, R. Phenylureas. Part 1. Mechanism of the basic hydrolysis of phenylureas. *J. Chem. Soc., Perkin Trans. 2* **2001**, 2226–2229.
(18) Laudien, R.; Mitzner, R. Phenylureas. Part 2. Mechanism of the acid hydrolysis of phenylureas. *J. Chem. Soc., Perkin Trans. 2* **2001**, 2230–2232.
(19) Gangwar, S. K.; Rafiquee, M. Z. A. Kinetics of the alkaline hydrolysis of isoproturon in CTAB and NaLS micelles. *Int. J. Chem. Kinet.* **2007**, *39*, 39–45.
(20) O'Connor, C. J.; Barnett, J. W. Acid hydrolysis of phenylurea, 4-fluorophenylurea, and 3-methylphenylurea. *J. Chem. Soc., Perkin Trans. 2* **1973**, 1457–1461.
(21) Penning, H.; Elsner, M. Intramolecular carbon and nitrogen isotope analysis by quantitative dry fragmentation of the phenylurea herbicide isoproturon in a combined injector/capillary reactor prior to GC separation. *Anal. Chem.* **2007**, *79*, 8399–8405.
(22) Adamo, C.; Barone, V. Exchange functionals with improved long-range behavior and adiabatic connection methods without adjustable parameters: The mPW and mPW1PW models. *J. Chem. Phys.* **1998**, *108*, 664–675.
(23) Perdew, J.; Wang, Y. Accurate and simple analytic representation of the electron-gas correlation energy. *Phys. Rev. B* **1992**, *45*, 13244–13249.
(24) Perdew, J. P. Unified Theory of Exchange and Correlation Beyond the Local Density Approximation In *Electronic Structure of Solids*; Ziesche, P., Eschrig, H. ,Eds.; Akademie Verlag: Berlin, 1991; pp 11−20.
(25) Hehre, W. J.; Radom, L.; Schleyer, P. v. R.; Pople, J. A. *Ab Initio Molecular Orbital Theory*; Wiley: New York, 1986.
(26) Cramer, C. J. *Essentials of Computational Chemistry: Theories and Models*, 2nd ed.; John Wiley & Sons: Chichester, 2004.
(27) Cramer, C. J.; Truhlar, D. G. Implicit solvation models: equilibria, structure, spectra, and dynamics. *Chem. Rev.* **1999**, *99*, 2161–2200.
(28) Frisch, M. J.; Trucks, G. W.; Schlegel, H. B.; Scuseria, G. E.; Robb, M. A.; Cheeseman, J. R.; Montgomery, J. A., Jr.; Vreven, T.; Kudin, K. N.; Burant, J. C.; Millam, J. M.; Iyengar, S. S.; Tomasi, J.; Barone, V.; Mennucci, B.; Cossi, M.; Scalmani, G.; Rega, N.; Petersson, G. A.; Nakatsuji, H.; Hada, M.; Ehara, M.; Toyota, K.; Fukuda, R.; Hasegawa, J.; Ishida, M.; Nakajima, T.; Honda, Y.; Kitao, O.; Nakai, H.; Klene, M.; Li, X.; Knox, J. E.; Hratchian, H. P.; Cross, J. B.; Bakken, V.; Adamo, C.; Jaramillo, J.; Gomperts, R.; Stratmann, R. E.; Yazyev, O.; Austin, A. J.; Cammi, R.; Pomelli, C.; Ochterski, J. W.; Ayala, P. Y.; Morokuma, K.; Voth, G. A.; Salvador, P.; Dannenberg, J. J.; Zakrzewski, V. G.; Dapprich, S.; Daniels, A. D.; Strain, M. C.; Farkas, O.; Malick, D. K.; Rabuck, A. D.; Raghavachari, K.; Foresman, J. B.; Ortiz, J. V.; Cui, Q.; Baboul, A. G.; Clifford, S.; Cioslowski, J.; Stefanov, B. B.; Liu, G.; Liashenko, A.; Piskorz, P.; Komaromi, I.; Martin, R. L.; Fox, D. J.; Keith, T.; Al-Laham, M. A.; Peng, C. Y.; Nanayakkara, A.; Challacombe, M.; Gill, P. M. W.; Johnson, B.; Chen, W.; Wong, M. W.; Gonzalez, C.; Pople, J. A. *Gaussian 03, revision C.02*; Gaussian, Inc.: Wallingford, CT, 2004.
(29) Rosell, M.; Barcelo, D.; Rohwerder, T.; Breuer, U.; Gehre, M.; Richnow, H. H. Variations in 13C/12C and D/H enrichment factors of aerobic bacterial fuel oxygenate degradation. *Environ. Sci. Technol.* **2007**, *41*, 2036–2043.

ES801101C